


Dominance of double processes in complete Auger decay of $\text{Rb}^+(3d^{-1})$ Liping Liu¹, Yongjun Li¹, Cheng Gao¹, and Jiaolong Zeng^{1,2,*}¹*Department of Physics, College of Liberal Arts and Sciences, National University of Defense Technology, Changsha Hunan, 410073, People's Republic of China*²*College of Science, Zhejiang University of Technology, Hangzhou 310023, People's Republic of China* (Received 1 October 2019; revised manuscript received 8 December 2019; published 13 January 2020)

The complete Auger decay of $\text{Rb}^+(3d^{-1})$ including single and double processes is investigated using the distorted wave approximation. The direct double Auger decay was calculated by separating the knock-out and shake-off mechanisms. For single Auger decay of the $3d^{-1}$ hole state, it is generally believed that the dominant channels should be levels belonging to the configurations of $[1s^22s^22p^63s^23p^63d^{10}]4s^24p^45s$, $4s4p^55s$, and $4s^04p^65s$. Here we predict that the strongest channels originate from $4s^24p^34d5s$, which accounts for 36.3% of the single Auger decay rate. The levels belonging to this configuration can further decay to Rb^{3+} , resulting in a large fraction of cascade double Auger decay. Moreover, the probability of direct double Auger decay in Rb is also high because of its 5s electron. The branching ratios of cascade and direct double Auger decay are predicted to be 50.60% and 22.13%, respectively, resulting in the dominance of double Auger decay with a fraction of 72.73% in the complete Auger decay of $\text{Rb}^+(3d^{-1})$.

DOI: [10.1103/PhysRevA.101.012507](https://doi.org/10.1103/PhysRevA.101.012507)**I. INTRODUCTION**

Single Auger decay (SAD) happens when an inner valence vacancy forms and an outer-shell electron fills the vacancy, emitting an Auger electron. Double Auger decay (DAD) [1–4] and triple Auger decay [5,6] can also happen if energetically allowed. In DAD, the two Auger electrons can be emitted sequentially or simultaneously, resulting in cascade double Auger decay (CDAD) or direct double Auger decay (DDAD). The higher-order DDAD process is caused only by electron correlation, and understanding this correlation helps to control multielectron processes [7]. Investigating DDAD requires a sophisticated theoretical methodology and a model that fully considers electron correlation [8–10]. Thus studying direct higher-order Auger decay is challenging.

The ground state of the alkali metal rubidium $[\text{Ar}]3d^{10}4s^24p^65s$ (where $[\text{Ar}]$ means $1s^22s^22p^63s^23p^6$) has a 5s electron in the outermost shell and an inner 4d shell, which affects the overlapping of the wave functions of the initial and final Auger decay states. Unfortunately, there is little research on the Auger decay of the open-shell atoms of $\text{Rb}^+(3d^{-1})$ [11,12] compared with the closed shell atoms (such as Ne [13,14], Ar [15], Kr [16,17], and Xe [18]). Aksela *et al.* [11] experimentally studied the $\text{M}_{4,5}\text{NO}$ and $\text{M}_{4,5}\text{NN}$ Auger decay of Rb to understand how the outermost 5s electron affected the hole states. To explain their experiment, they also performed extensive multiconfiguration Dirac-Fock (MCDF) calculations, which revealed the importance of the 5s electron on the electron correlation of the final Auger states. They stated that even the most elaborate configuration interaction (CI) calculations failed to identify the observed spectra. Very recently, Keskinen and co-workers [12] investigated the Auger decay of these states by using a photoelectron-Auger

electron coincidence measurement. Also, 3d photoionization and subsequent Auger decay of $\text{Rb}^+(3d^94s^24p^65p)$ have been investigated experimentally and theoretically [19]. The KLL Auger spectrum of rubidium has been studied by Inoyatov [20]. However, the research was limited to SAD and no research has been reported on the DDAD of $\text{Rb}^+(3d^{-1})$, to the best of our knowledge. Triple Auger decay is not relevant here, because the energy of $\text{Rb}^+(3d^{-1})$ is not high enough to undergo it, either in cascade or direct processes.

The extra 5s electron in the outermost shell of Rb versus Kr ($[\text{Ar}]3d^{10}4s^24p^6$) produces new features in its $3d^{-1}$ Auger decay. First, the treatment of the electron correlation in $\text{Rb}^+(3d^{-1})$ is much more complicated than in $\text{Kr}^+(3d^{-1})$, as mentioned above. Second, the dominant Auger decay channels are qualitatively and quantitatively different. It is generally believed that the dominant Auger decay channels should be quantum states of the configurations of $4p^{-2}$, $4s^{-1}4p^{-1}$, and $4s^{-2}$. For $\text{Kr}^+(3d^{-1})$, this idea roughly holds. For $\text{Rb}^+(3d^{-1})$, however, this idea is untenable. Finally, the branching ratio (BR) of DAD of $\text{Rb}^+(3d^{-1})$ is much larger than that of $\text{Kr}^+(3d^{-1})$, whereas $\text{Rb}^+(3d^{-1})$ is reversed, with DAD dominating its total Auger decay.

In this work, we investigated the complete Auger decay, including single and double processes of $\text{Rb}^+(3d^{-1})$ at the fine-structure level, using the distorted wave approximation. The DDAD rates are computed using the theoretical framework of the separation of knock-out (KO) and shake-off (SO) mechanisms [8]. The CI calculation was done at large scale in order to obtain results that are as accurate as possible. The calculated natural lifetime width and SAD spectra are compared with available experimental and theoretical results [12].

II. THEORETICAL METHOD

The calculation of Auger decay was carried out using the perturbation theory, implemented by the distorted wave

*jlzeng@nudt.edu.cn

approximation using the flexible atomic code (FAC) developed by Gu [21]. Accurate wave functions are required for the three successive ionization stages of Rb^+ , Rb^{2+} , and Rb^{3+} in order to obtain accurate DDAD rates. A complete description of this theoretical formalism can be found in previous work [22–24], but a brief outline is given as follows.

In first-order perturbation theory, the SAD rate can be written as (atomic units are used in this section) [21,25]

$$A_{im}^1 = 2 \left| \langle \Psi_m^+ | \sum_{i < j} \frac{1}{r_{ij}} | \Psi_i \rangle \right|^2, \quad (1)$$

where $|\Psi_i\rangle$ and $|\Psi_m^+\rangle$ are the wave functions of the initial and Auger ionic states (plus a free electron). The CDAD rates are determined by two steps of SAD of Rb^+ and Rb^{2+} .

The DDAD rates are obtained in second-order perturbation theory as

$$A_{if}^2 = \frac{8}{\pi} \int_0^{k_{\max}} \frac{dk_{f1}}{k_{f2}} \times \left| \sum_m \sum_{k_m} \frac{\langle \Psi_f^{2+} | \sum_{i < j} \frac{1}{r_{ij}} | \Psi_m^+ \rangle \langle \Psi_m^+ | \sum_{i < j} \frac{1}{r_{ij}} | \Psi_i \rangle}{\varepsilon_i - \varepsilon_m^+ - k_m^2/2} \right|^2, \quad (2)$$

where $|\Psi_f^{2+}\rangle$ is the wave function of the final state with a charge $q + 2$ plus two continuum electrons. The total energy $E = \varepsilon_f^{2+} + E_{\max}$ is conserved with that of the initial level $E = \varepsilon_i$, where $E_{\max} = k_{f1}^2/2 + k_{f2}^2/2$ with k_{f1} and k_{f2} being the momenta of the two Auger electrons. To simplify the DDAD calculations, we used the generally agreed-on mechanisms of shake-off and knock-out [8]. The rates of KO and SO mechanism can be written as

$$A_{\text{KO}}^2 = \sum_m A_{im}^1 \sigma_{mf}(\varepsilon_0) \quad (3)$$

and

$$A_{\text{SO}}^2 = \sum_m A_{im}^1 |\langle \Psi_f^{2+} | \Psi_m \rangle|^2, \quad (4)$$

where A_{im}^1 is the single Auger decay rate from the initial hole level i to a middle level m and $\sigma_{mf}(\varepsilon_0)$ is the cross section of the inelastic scattering of the intermediate Auger electron from the middle level m to the final level f .

To properly describe the electron correlations, large-scale CI calculations were done to obtain the single and double Auger decay rates for the hole states of $3d^9 4s^2 4p^6 5s$ in Rb^+ . For Rb^+ , we included the interactions among the fine-structure levels belonging to the following configurations: $3d^{10} 4s^2 4p^6$, $3d^{10} 4s^2 4p^5 nl$, $3d^{10} 4s 4p^6 nl$, $3d^{10} 4s^2 4p^4 4d nl$, $3d^{10} 4s^2 4p^4 5s nl$, $3d^{10} 4s^2 4p^4 5p^2$, $3d^{10} 4s^2 4p^4 5d^2$, $3d^{10} 4s 4p^5 4d nl$, $3d^{10} 4s 4p^5 5s nl$, $3d^9 4s^2 4p^6 nl$, $3d^9 4s^2 4p^5 5s nl$, $3d^9 4s 4p^6 5s nl$, $3d^9 4s^2 4p^4 4d 5s^2$, and $3d^9 4s^2 4p^4 4d^2 5s$ ($nl = 4d, 4f, 5s, 5p, 5d, 5f, 6s, 6p, 6d$). The same scale of CI was applied to Rb^{2+} and Rb^{3+} . In short, we performed calculations that includes the electron correlations among the singly and doubly excitations from the respective ground configurations

TABLE I. The final levels, angular momenta J , energies (in eV) relative to the ground level of $\text{Rb}^+(4s^2 4p^6)$, transition energies ΔE (in eV) and rates A^1 (s^{-1}) for the SAD of $\text{Rb}^+(3d_{5/2}^{-1} 5s_{1/2})_3$ hole state. To save space, only stronger channels with rates larger than $1.0 \times 10^{12} \text{ s}^{-1}$ are given. Figures in square brackets indicate powers of ten.

Final level	J	Energy	ΔE	A^1
$4s^2[(4p_{1/2} 4p_{3/2})_2 4d_{5/2}^2]_0 5s_{1/2}$	1/2	107.47	5.75	2.418[12]
$[4s_{1/2} 4p_{1/2}^2(4p_{3/2}^2)_{3/2}]_2 5s_{1/2}$	5/2	65.93	47.59	1.755[12]
$[(4s_{1/2} 4p_{1/2}^2)_0 4p_{3/2}^2]_2 5s_{1/2}$	3/2	66.12	47.19	3.359[12]
$[(4s_{1/2} 4p_{1/2})_0 4p_{3/2}^4]_0 5s_{1/2}$	1/2	66.70	46.83	2.534[12]
$(4s_{1/2} 4p_{1/2} 4p_{3/2}^2)_0 5s_{1/2}$	1/2	67.52	45.72	1.700[12]
$4s^2[(4p_{1/2} 4p_{3/2}^2)_{5/2} 4d_{5/2}]_{5/2} 5s_{1/2}$	3/2	70.01	43.22	9.465[12]
$4s^2[(4p_{1/2} 4p_{3/2}^2)_{5/2} 4d_{5/2}]_1 5s_{1/2}$	3/2	70.10	43.15	1.032[13]
$4s^2(4p_{1/2} 4p_{3/2}^2)_{3/2} 4d_{5/2}^2$	1/2	77.50	35.73	1.232[12]
$4s^2(4p_{3/2}^3 4d_{5/2})_1 5s_{1/2}$	3/2	78.00	35.21	1.562[12]
$4s^2[(4p_{1/2} 4p_{3/2}^2)_{1/2} 4d_{3/2}]_1 5s_{1/2}$	3/2	78.86	34.36	2.760[12]
$(4s_{1/2} 4p_{1/2}^2 4p_{3/2}^2)_1 5s_{1/2}$	1/2	78.87	34.34	1.193[13]
$4s^2(4p_{3/2}^3 4d_{3/2})_1 5s_{1/2}$	3/2	79.11	34.10	5.832[12]
$4s^2 4p_{1/2} (4p_{3/2}^2)_0 5s^2$	1/2	79.77	33.45	1.846[12]
$4s^2(4p_{3/2}^3 4d_{5/2})_1 5s_{1/2}$	1/2	81.37	31.84	1.630[12]
$4s^0 4p^6 5s_{1/2}$	1/2	86.75	26.47	6.490[12]
$[(4s_{1/2} 4p_{3/2}^2 4p_{3/2}^2)_0 4d_{3/2}]_2 4d_{5/2}$	1/2	98.71	14.51	1.582[12]
$[(4s_{1/2} 4p_{1/2}^2 4p_{3/2}^2)_{3/2} 4d_{3/2}]_2 4d_{5/2}$	1/2	99.08	14.13	1.322[12]
$4s^2(4p_{1/2} 4p_{3/2}^3)_2 5s_{1/2}$	5/2	51.27	61.95	6.342[12]
$4s^2(4p_{1/2} 4p_{3/2}^3)_2 5s_{1/2}$	3/2	51.54	61.94	5.562[12]
$4s^2 4p^4 5s_{1/2}$	1/2	53.50	59.79	1.254[12]
$4s^2(4p_{1/2} 4p_{3/2}^3)_2 4d_{5/2}$	1/2	53.30	57.92	1.130[12]
All possible channels				1.246[14]

of Rb^+ , Rb^{2+} , and Rb^{3+} to the pathways of $4d$, $4f$, $5s$, $5p$, $5d$, $5f$, $6s$, $6p$, and $6d$.

III. RESULTS AND DISCUSSION

A. Single Auger decay

We first investigate the SAD of the four fine-structure levels of $(3d_{5/2}^{-1} 5s_{1/2})_{3,2}$ (which means $(3d_{5/2}^{-1} 5s_{1/2})_3$ and $(3d_{5/2}^{-1} 5s_{1/2})_2$) and $(3d_{3/2}^{-1} 5s_{1/2})_{1,2}$ (which means $(3d_{3/2}^{-1} 5s_{1/2})_1$ and $(3d_{3/2}^{-1} 5s_{1/2})_2$) belonging to $\text{Rb}^+(3d^{-1} 5s)$. To save space, the stronger decay channels are given in Table I with rates larger than $1.0 \times 10^{12} \text{ s}^{-1}$ for the level of $(3d_{5/2}^{-1} 5s_{1/2})_3$. We found that multiple decay pathways are possible for this Auger process, which is much more complicated than those of closed-shell atoms [13–17]. There are two very strong channels with rates larger than $1.0 \times 10^{13} \text{ s}^{-1}$, which are designated as $[4s^2((4p_{1/2} 4p_{3/2}^2)_{5/2} 4d_{5/2})_1 5s_{1/2}]_{3/2}$ ($1.032 \times 10^{13} \text{ s}^{-1}$) and $[(4s_{1/2} 4p_{1/2}^2 4p_{3/2}^2)_1 5s_{1/2}]_{1/2}$ ($1.193 \times 10^{13} \text{ s}^{-1}$).

Figures 1 and 2 show the Auger electron spectra of $\text{Rb}^+(3d_{5/2}^{-1})$ and $\text{Rb}^+(3d_{3/2}^{-1})$, respectively. These figures were produced by statistically averaging the Auger spectra of the $(3d_{5/2}^{-1} 5s_{1/2})_3$ and $(3d_{5/2}^{-1} 5s_{1/2})_2$ levels for $\text{Rb}^+(3d_{5/2}^{-1})$, as well

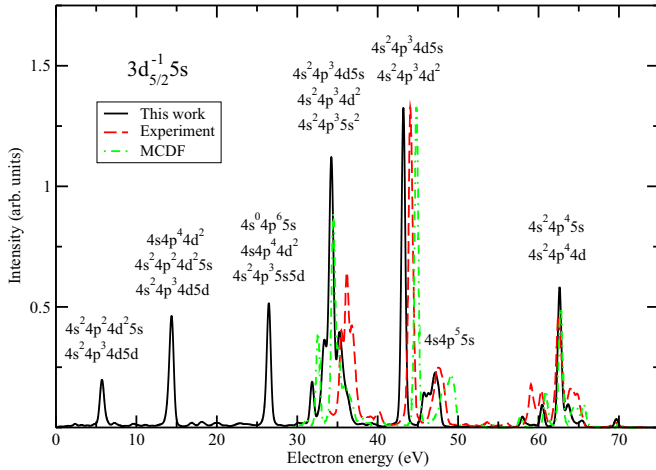


FIG. 1. Auger electron spectra for single Auger decay of $\text{Rb}^+(3d_{5/2}^{-1})$ compared with experiment [12] and MCDF calculation [12].

as $(3d_{3/2}^{-1}5s_{1/2})_1$ and $(3d_{3/2}^{-1}5s_{1/2})_2$ levels for $\text{Rb}^+(3d_{3/2}^{-1})$. The Auger electron spectra were calculated according to natural lifetime broadening with a Lorentzian profile

$$I(E) = \frac{2}{\pi} \frac{\Gamma_l}{\Gamma_l^2 + 4(E - E_0)^2}, \quad (5)$$

where $I(E)$ is the intensity of the Auger electron with a kinetic energy E , Γ_l is the Lorentzian full width at half maximum (FWHM), and E_0 is the central energy of the Auger transition. The dominant pathways are identified and marked in the figures. The strongest peak, near 45 eV, originates mostly from the levels of configuration $4s^2 4p^3 4d 5s$, although the levels of $4s^2 4p^3 4d^2$ contribute somewhat. The second strongest peak, near 35 eV, also originates mostly from the levels of configuration $4s^2 4p^3 4d 5s$, with some contributions from $4s^2 4p^3 4d^2$ and $4s^2 4p^3 5s^2$. Here, the Auger channels of $4s^2 4p^4 5s$, $4s 4p^5 5s$, and $4s^0 4p^6 5s$, which are generally believed strong, are much weaker than those of $4s^2 4p^3 4d 5s$.

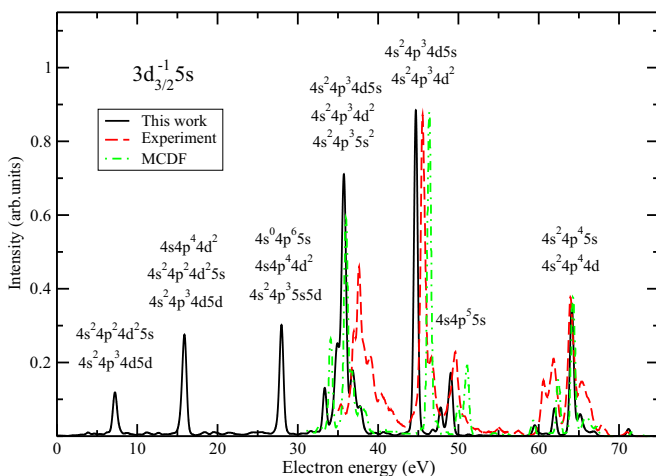


FIG. 2. Auger electron spectra for single Auger decay of $\text{Rb}^+(3d_{3/2}^{-1})$ compared with experiment [12] and MCDF [12].

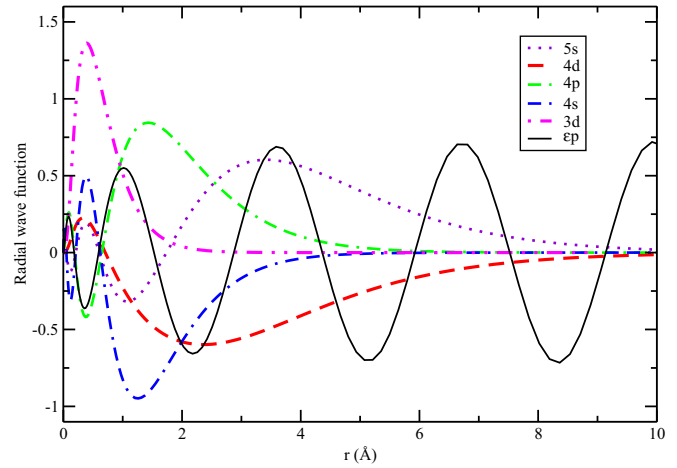


FIG. 3. Radial wave functions of the bound electrons of $5s$ (violet dotted line), $4d$ (red dashed line), $4p$ (green dotted-dashed line), $4s$ (blue dotted-dashed-dashed line), $3d$ (magenta dotted-dotted-dashed line), and the continuum electron ϵp (solid black line). The continuum electron is ejected from the Auger decay channel of $(3d_{5/2}^{-1}5s_{1/2})_3 \rightarrow 4s^2[(4p_{1/2}4p_{3/2}^2)_{5/2}4d_{5/2}5/25s_{1/2}]_{3/2} + \epsilon p$, with a kinetic energy of 43.3 eV.

The reason for the strongest Auger decay channels originating from the levels of $4s^2 4p^3 4d 5s$ can be understood from the definition of Auger decay rate [see Eq. (1)], which is determined by the transition matrix element of Coulombic interaction among electrons over the initial and final states. From the definition, we know that the Auger decay is completely caused by electron correlation among the bound and continuum electrons. Besides the definite overlapping of the wave functions of angular parts, the decay channels are closely related with the radial wave functions. In Fig. 3, we show the radial wave functions of the bound electrons of $5s$, $4d$, $4p$, $4s$, and $3d$ and continuum electron ejected from the Auger decay channel of $(3d_{5/2}^{-1}5s_{1/2})_3 \rightarrow 4s^2[(4p_{1/2}4p_{3/2}^2)_{5/2}4d_{5/2}5/25s_{1/2}]_{3/2} + \epsilon p$. From the inspection of this figure, we find that the wave functions of $4s$ and $4p$ electrons do have a strong overlapping with the continuum electron and thus the Auger channels of $4s^2 4p^4 5s$, $4s 4p^5 5s$, and $4s^0 4p^6 5s$ belong to the stronger channels. However, stronger correlation between $4d$ and $5s$ electrons and the continuum electron than that of $4s$ and $4p$ is found. As shown in Fig. 3, $4s$ and $4p$ electrons are more localized in a smaller distance r from the nucleus and more localized in a smaller spatial range. Meanwhile, the amplitude of the continuum wave function is smaller at a smaller r and with increasing r , the amplitude of the continuum wave function increases until reaching a steady value with an equivalent amplitude. This is a common feature of distorted ionic potential. Unlike the $4s$ and $4p$ electrons, the wave functions of $4d$ and $5s$ maximize their value of amplitude at a larger r and expand in a much wider spatial range. Therefore the integral of Eq. (1) over the physical space is larger between the $4d$ and $5s$ and continuum electron than that of the $4s$ and $4p$ electrons. As a result, the Auger decay rate originating from levels belonging to the configuration of $4s^2 4p^3 4d 5s$ is larger than those of $4s^2 4p^4 5s$, $4s 4p^5 5s$, and $4s^0 4p^6 5s$ configurations.

TABLE II. The level-to-configuration rates (s^{-1}) and BRs (in percent) for the SAD of initial levels of $(3d_{5/2}^{-1}5s_{1/2})_3$ (a), $(3d_{5/2}^{-1}5s_{1/2})_2$ (b), $(3d_{3/2}^{-1}5s_{1/2})_1$ (c), and $(3d_{3/2}^{-1}5s_{1/2})_2$ (d). Only those with a value of BR larger than 1.0% are given. The configuration-averaged results of $3d^{-1}5s$ (f) are compared with previous theoretical work [11]. Figures in square brackets indicate powers of ten.

Final config.	Rate						Ref. [11]	BR					
	a	b	c	d	f	a		b	c	d	f	Ref. [11]	
$4s^24p^5$	1.530[12]	2.635[12]	1.390[12]	2.299[12]	1.977[12]	1.321[12]		1.2	2.1	1.2	1.9	1.6	1.4
$4s^24p^44d$	2.367[12]	2.208[12]	2.798[12]	2.228[12]	2.357[12]	–		1.9	1.8	2.3	1.8	2.0	–
$4s^24p^45s$	1.471[13]	1.463[13]	1.470[13]	1.516[13]	1.480[13]	2.498[13]		11.8	11.7	12.2	12.6	12.3	20.8
$4s4p^55s$	2.155[13]	7.286[12]	6.648[12]	1.635[13]	1.445[13]	7.350[13]		17.3	5.8	5.5	13.6	12.0	61.2
$4s^04p^65s$	1.205[13]	1.216[13]	1.139[13]	1.140[13]	1.182[13]	1.838[13]		9.7	9.7	9.5	9.5	9.8	15.3
$4s^24p^34d^2$	5.564[12]	5.839[12]	4.733[12]	4.397[12]	5.217[12]	–		4.5	4.7	3.9	3.6	4.3	–
$4s^24p^34d5s$	3.925[13]	4.881[13]	5.192[13]	3.952[13]	4.361[13]	–		31.5	39.1	43.1	32.8	36.3	–
$4s^24p^35s5d$	1.576[12]	1.297[12]	1.401[12]	1.397[12]	1.435[12]	–		1.3	1.0	1.2	1.2	2.1	–
$4s4p^44d^2$	3.563[12]	3.415[12]	3.151[12]	3.242[12]	3.384[12]	–		2.9	2.7	2.6	2.7	2.2	–
$4s4p^44d5d$	2.022[12]	2.091[12]	2.035[12]	2.020[12]	2.041[12]	–		1.6	1.7	1.7	1.7	1.6	–
$4s^24p^24d^25s$	6.008[12]	5.905[12]	5.737[12]	5.810[12]	5.892[12]	–		4.8	4.7	4.8	4.8	3.6	–
$4s^24p^35s^2$	3.449[12]	5.879[12]	2.310[12]	5.059[12]	4.288[12]	–		2.7	4.7	1.9	4.2	3.0	–
Total	1.136[14]	1.122[14]	1.082[14]	1.089[14]	1.113[14]	1.185[14]		91.2	89.7	89.9	90.4	90.8	98.7

As shown in Figs. 1 and 2, our theoretical Auger electron spectra are compared with available experimental and theoretical results [12]. The theoretical results are MCDF calculations using the atomic structure code GRASP2K [26,27] and the RELCI component of the RATIP package [28,29]. To compare it with experimental data, we considered instrumental broadening in our spectra. As shown in both figures, our calculated SAD electron spectra agree well with the available theoretical results [12]. Both theoretical calculations reasonably explain the experimental results [12]. In particular, the energy positions and relative intensities of the Auger channels of $4s^24p^45s$ and $4s4p^55s$ are in good agreement with the experimental measurement. In the electron energy range of 30–40 eV, however, the energy locations predicted by both theoretical calculations are about 2 eV smaller than those of the experiment, and the theoretical peak intensity is higher than that of the experiment. Thus both theories predicted energy levels of the $4s^24p^34d5s$ configuration that were 2 eV higher than the experimental results. Although we did a large-scale CI calculation, the electron correlations for the levels of $4s^24p^34d5s$ are still inadequate to obtain a converged result. According to our calculation, the energy is in the range of 65.62–67.49 eV for the levels of $4s4p^55s$, but it is in the range of 68.57–81.36 eV (with an interval of 12.79 eV) for the levels of $4s^24p^34d5s$. This result indicates strong CI for the Auger decay of $Rb^+(3d^{-1})$, which requires the inclusion of enough electronic correlations, as demonstrated in investigations of Auger decay [30,31] and photoionization processes [32]. With a large energy interval and correlations with many more highly excited states, adequate description of $4s^24p^34d5s$ requires the inclusion of more electron correlation from levels with higher energies than those of $4s^24p^34d5s$.

To better understand the Auger decay channels, Table II shows the level-to-configuration rates and BRs of the dominant pathways of the four fine-structure levels of $Rb^+(3d^{-1})$.

The largest BR originates from $4s^24p^34d5s$, which contributes to the two strongest structures near 45 and 35 eV. The next strongest Auger electron spectra get contributions from $4s^24p^45s$, $4s4p^55s$, and $4s^04p^65s$, accounting for $\approx 12\%$, $\approx 12\%$, and $\approx 10\%$, respectively. Generally, it is believed that the dominant Auger decay channels for the SAD of $Rb^+(3d^{-1})$ should be levels of $4s4p^55s$, $4s^24p^45s$, and $4s^04p^65s$. Here we predict that the largest BR originates from $4s^24p^34d5s$, which accounts for 31.5%, 39.1%, 43.1%, and 32.8% for the four initial levels of $Rb^+(3d^{-1})$. The calculated lifetime of $Rb^+(3d^{-1})$ is 81.0 meV, close to the experimental value of 79.0 meV [11].

Aksela *et al.* [11] reported the Auger decay rates for the configuration averaged results of $Rb^+(3d^{-1})$, which were obtained by summing all possible final states and then averaging over the initial states of $(3d_{5/2}^{-1}5s_{1/2})_{3,2}$ and $(3d_{3/2}^{-1}5s_{1/2})_{1,2}$. We compare these data with our results in Table II. The largest discrepancy is in the BR of $4s4p^55s$, with 61.2% in the previous work [11] and only 12.0% here. This is because Aksela *et al.* attributed the contribution of $4s^24p^34d5s$ to $4s4p^55s$ [11], while we predict a BR of 36.3% for the configuration of $4s^24p^34d5s$. Summing the $4s4p^55s$ and $4s^24p^34d5s$ configurations accounts for a BR of 48.3%, which is much closer to the BR predicted by Aksela *et al.* [11].

B. Double Auger decay

The calculated first ionization potentials of Rb^+ and Rb^{2+} are 27.11 and 38.78 eV, respectively, which are close to the values of 27.29 and 39.25 eV from NIST [33]. The energy to ionize Rb^+ to Rb^{3+} is at least 66.54 eV [33]. The binding energy of $Rb^+(3d^{-1})$ is 117.4 eV [11], while the energy to ionize Rb^+ to Rb^{4+} is at least 118.74 eV [33]. Thus the triple Auger decay of $Rb^+(3d^{-1})$ is energetically forbidden.

TABLE III. The final levels, angular momenta J , transition energies ΔE (in eV) and rates A_{CDAD}^2 (s^{-1}) for the CDAD of $\text{Rb}^+(3d_{5/2}^{-1}5s_{1/2})_{3,2}$ hole states. Only stronger channels with rates larger than $1.0 \times 10^{12} \text{ s}^{-1}$ are given. Figures in square brackets indicate powers of ten.

Initial level	Final level	J	ΔE	A_{CDAD}^2
$(3d_{5/2}^{-1}5s_{1/2})_3$	$4s^2(4p_{1/2}^2)_{2,4}p_{3/2}^2$	2	48.57	1.122[13]
	$4s^24p_{1/2}(4p_{3/2}^3)_{3/2}$	1	47.87	1.480[13]
	$4s^24p_{1/2}(4p_{3/2}^3)_{3/2}$	2	46.22	2.157[13]
	$4s^2(4p_{1/2}^2)_{0,4}p_{3/2}^2$	0	47.74	5.367[12]
	$4s^2(4p_{3/2}^4)_0$	0	43.71	3.666[12]
	$4s_{1/2}4p_{1/2}^2(4p_{3/2}^3)_{3/2}$	2	31.83	3.879[12]
	$4s_{1/2}4p_{1/2}(4p_{3/2}^4)_0$	1	31.31	2.246[12]
	$4s_{1/2}4p_{1/2}^2(4p_{3/2}^3)_{3/2}$	1	27.23	1.663[12]
	$4s^2(4p_{3/2}^3)_{3/2}4d_{5/2}$	3	20.16	1.761[12]
	$4s^2(4p_{3/2}^3)_{3/2}4d_{3/2}$	3	16.98	1.589[12]
All possible channels				8.480[13]
$(3d_{5/2}^{-1}5s_{1/2})_2$	$4s^24p_{1/2}(4p_{3/2}^3)_{3/2}$	1	47.92	1.182[13]
	$4s^24p_{1/2}(4p_{3/2}^3)_{3/2}$	2	46.27	1.897[13]
	$4s^2(4p_{1/2}^2)_{2,4}p_{3/2}^2$	2	48.61	9.373[12]
	$4s^2(4p_{1/2}^2)_{0,4}p_{3/2}^2$	0	47.79	3.700[12]
	$4s^2(4p_{3/2}^4)_0$	0	43.76	2.961[12]
	$4s_{1/2}4p_{1/2}^2(4p_{3/2}^3)_{3/2}$	2	31.88	3.858[12]
	$4s_{1/2}4p_{1/2}(4p_{3/2}^4)_0$	1	31.35	2.272[12]
	$4s_{1/2}4p_{1/2}^2(4p_{3/2}^3)_{3/2}$	1	27.28	1.660[12]
	$4s^2(4p_{3/2}^3)_{3/2}4d_{5/2}$	3	20.20	1.767[12]
	$4s^2(4p_{3/2}^3)_{3/2}4d_{3/2}$	3	17.03	1.586[12]
All possible channels				7.497[13]

Because of its extra outermost $5s$ electron, most of the final states in SAD of $\text{Rb}^+(3d^{-1})$ can Auger decay further to the higher ionization stage of Rb^{3+} by cascade processes. As shown in Figs. 1 and 2, the corresponding Auger ionic states with Auger electron energy less than 48 eV are energetically allowed to undergo CDAD. Thus, the levels belonging to the configurations of $4s^24p^34d5s$, $4s^24p^34d^2$, $4s^24p^35s^2$, $4s^04p^65s$, $4s4p^44d^2$, $4s^24p^35s5d$, $4s^24p^24d^25s$, and $4s^24p^34d5d$ can further decay to Rb^{3+} . The generally believed stronger Auger decay channels originating from levels belonging to the configurations of $4s^24p^45s$ and $4s4p^55s$ have no pathways to further decay to Rb^{3+} by cascade Auger processes. Table III shows the stronger CDAD channels with rates larger than $1.0 \times 10^{12} \text{ s}^{-1}$ for the initial states of $(3d_{5/2}^{-1}5s_{1/2})_{3,2}$. Our calculated total CDAD rates are 8.480×10^{13} , 7.497×10^{13} , 7.146×10^{13} , and $8.316 \times 10^{13} \text{ s}^{-1}$ for the initial states of $(3d_{5/2}^{-1}5s_{1/2})_{3,2}$ and $(3d_{3/2}^{-1}5s_{1/2})_{1,2}$, compared with the total SAD rates of 1.264×10^{14} , 1.248×10^{14} , 1.205×10^{14} , and $1.205 \times 10^{14} \text{ s}^{-1}$. As shown in Table III, the predominant CDAD channels are levels of the ground configuration $4s^24p^4$ and the first excited configuration $4s^24p^34d$ of Rb^{3+} , with BRs in the total CDAD process of 66.7% and 14.6%, respectively. Since the energies of the dominant SAD production of the first step such as $4s^24p^34d5s$, are

TABLE IV. The final levels, angular momenta J , transition energies ΔE (in eV) and rates A_{DDAD}^2 (s^{-1}) for the DDAD of $\text{Rb}^+(3d_{5/2}^{-1}5s_{1/2})_{3,2}$ hole states. Only stronger channels with rates larger than $5.0 \times 10^{11} \text{ s}^{-1}$ are given. Figures in square brackets indicate powers of ten.

Initial level	Final level	J	ΔE	A_{DDAD}^2	
$(3d_{5/2}^{-1}5s_{1/2})_3$	$4s^24p_{1/2}(4p_{3/2}^3)_{3/2}$	2	46.22	2.365[12]	
	$4s_{1/2}4p_{1/2}^2(4p_{3/2}^3)_{3/2}$	2	31.83	2.662[12]	
	$4s_{1/2}4p_{1/2}(4p_{3/2}^4)_0$	1	31.31	1.297[12]	
	$4s_{1/2}4p_{1/2}^2(4p_{3/2}^3)_{3/2}$	1	27.23	2.325[12]	
	$4s^2(4p_{1/2}4p_{3/2}^2)_{1/2}5s_{1/2}$	1	18.64	1.438[12]	
	$4s_{1/2}4p_{1/2}(4p_{3/2}^4)_0$	0	30.95	7.709[11]	
	$4s^2(4p_{3/2}^3)_{3/2}4d_{5/2}$	2	21.22	7.669[11]	
	$4s^2(4p_{1/2}4p_{3/2}^2)_{5/2}5s_{1/2}$	2	19.44	6.087[11]	
	$4s^04p_{1/2}^2(4p_{3/2}^4)_0$	0	10.88	8.889[11]	
	$4s^2(4p_{3/2}^3)_{3/2}4d_{5/2}$	3	20.16	5.528[11]	
$(3d_{5/2}^{-1}5s_{1/2})_2$	$4s^2(4p_{1/2}4p_{3/2}^2)_{5/2}5s_{1/2}$	2	19.64	5.291[11]	
	$4s^2(4p_{3/2}^3)_{3/2}4d_{3/2}$	1	18.34	5.604[11]	
	$4s^2(4p_{1/2}4p_{3/2}^2)_{3/2}4f_{5/2}$	2	10.18	5.971[11]	
	All possible channels				3.459[13]
	$(3d_{5/2}^{-1}5s_{1/2})_2$	$4s^24p_{1/2}(4p_{3/2}^3)_{3/2}$	2	46.27	2.188[12]
		$4s_{1/2}4p_{1/2}^2(4p_{3/2}^3)_{3/2}$	2	31.88	3.873[12]
		$4s_{1/2}4p_{1/2}(4p_{3/2}^4)_0$	1	31.35	1.049[12]
		$4s_{1/2}4p_{1/2}^2(4p_{3/2}^3)_{3/2}$	0	31.00	6.973[11]
		$4s_{1/2}4p_{1/2}^2(4p_{3/2}^3)_{3/2}$	1	27.28	9.177[11]
		$4s^2(4p_{3/2}^3)_{3/2}4d_{5/2}$	2	21.26	7.405[11]
$4s^2(4p_{3/2}^3)_{3/2}4d_{3/2}$		3	20.20	6.585[11]	
$4s^2(4p_{1/2}4p_{3/2}^2)_{5/2}5s_{1/2}$		2	19.49	5.702[11]	
$4s^2(4p_{1/2}4p_{3/2}^2)_{1/2}5s_{1/2}$		1	18.68	8.189[11]	
$4s^2(4p_{3/2}^3)_{3/2}4d_{3/2}$		1	18.39	9.583[11]	
$(3d_{5/2}^{-1}5s_{1/2})_2$	$4s^04p_{1/2}^2(4p_{3/2}^4)_0$	0	10.92	9.075[11]	
	$4s^2(4p_{1/2}4p_{3/2}^2)_{3/2}4f_{5/2}$	2	10.22	5.946[11]	
	All possible channels				3.506[13]

only slightly higher than the ionization threshold of further Auger decay, the final states of CDAD processes are predominantly levels belonging to the ground configuration $4s^24p^4$.

Table IV shows the level-to-level DDAD rates for the stronger channels of $(3d_{5/2}^{-1}5s_{1/2})_{3,2}$ with a rate larger than $5.0 \times 10^{11} \text{ s}^{-1}$. The direct double Auger electron spectra are shown in Fig. 4 for the four levels of $\text{Rb}^+(3d^{-1})$. The strongest DDAD channel is $[4s_{1/2}4p_{1/2}^2(4p_{3/2}^3)_{3/2}]_2$ for both levels of $(3d_{5/2}^{-1}5s_{1/2})_{3,2}$, with DDAD rates of 2.662×10^{12} and $3.873 \times 10^{12} \text{ s}^{-1}$, respectively. The strongest peak, in the energy range of 30–34 eV, gets contributions from the final levels belonging to the configuration $4s4p^5$. The strongest peak, in the energy range of 25–30 eV, comes mainly from the levels belonging to the configuration $4s^24p^34d$, with some contribution from $4s4p^5$.

Table V shows the level-to-configuration rates and BRs of the dominant final configurations for the DDAD processes

TABLE V. The level-to-configuration DDAD rates A_{DDAD}^2 (s^{-1}) and BRs (in percent %) of the initial levels $(3d_{5/2}^{-1}5s_{1/2})_3$ (a), $(3d_{5/2}^{-1}5s_{1/2})_2$ (b), $(3d_{3/2}^{-1}5s_{1/2})_1$ (c), and $(3d_{3/2}^{-1}5s_{1/2})_2$ (d) of Rb^+ for the stronger configurations of Rb^{3+} . Figures in square brackets indicate powers of ten.

Final config.	Rate				BR			
	a	b	c	d	a	b	c	d
$4s^24p^4$	2.311[12]	2.278[12]	2.132[12]	2.184[12]	8.5	8.2	7.8	7.9
$4s^24p^34d$	6.046[12]	7.131[12]	6.849[12]	6.015[12]	22.3	25.9	25.1	21.7
$4s^24p^34f$	2.800[12]	2.819[12]	2.604[12]	2.656[12]	10.3	10.3	9.5	9.6
$4s^24p^35s$	3.864[12]	3.327[12]	3.124[12]	3.902[12]	14.2	12.1	11.4	14.0
$4s^24p^35f$	6.307[11]	6.480[11]	8.934[11]	9.422[11]	2.3	2.4	3.3	3.4
$4s^24p^36p$	6.978[11]	7.836[11]	8.961[11]	9.017[11]	2.5	2.8	3.3	3.2
$4s4p^5$	5.531[12]	5.125[12]	5.096[12]	5.474[12]	20.4	18.6	18.7	19.7
$4s4p^44d$	3.237[12]	3.317[12]	3.519[12]	3.555[12]	11.9	12.1	12.9	12.8
$4s4p^45s$	9.276[11]	9.383[11]	1.028[12]	1.001[12]	3.4	3.4	3.8	3.6
$4s^04p^6$	6.969[11]	7.115[11]	6.890[11]	6.994[11]	2.6	2.6	2.5	2.5
Total	2.674[13]	2.708[13]	2.683[13]	2.733[13]	98.4	98.4	98.3	98.4

of $\text{Rb}^+(3d^{-1})$. For the four initial states of $\text{Rb}^+(3d^{-1})$, the decay rates to different final configurations are nearly equivalent except for $4s^24p^35f$ and $4s^24p^36p$. For these two configurations with a higher excited $5f$ or $6p$ electron, the decay rates of $(3d_{5/2}^{-1}5s_{1/2})_{3,2}$ are slightly smaller than those of $(3d_{3/2}^{-1}5s_{1/2})_{1,2}$. For each initial state, the strongest channel originates from $4s^24p^34d$, accounting for $\approx 22\%$. The next

strongest one is $4s4p^5$ with a BR of $\approx 19\%$. The next strongest channels belong to $4s^24p^35s$, $4s^24p^34f$, $4s4p^44d$, and $4s^24p^4$. The BRs of the ground configuration $4s^24p^4$ of Rb^{3+} are 8.5%, 8.2%, 7.8%, and 7.9%, for the four initial levels, respectively. This is different from the CDAD processes, where the fraction of the pathway to the ground configuration $4s^24p^4$ is $\approx 66.7\%$.

Table VI summarizes our results, including the Auger decay rates and BRs of SAD, DDAD, CDAD, and DAD of the four levels of $\text{Rb}^+(3d^{-1})$. For the four initial levels, the total SAD rates and DDAD rates are very close. The CDAD has a high BR, which accounts for 53.26%, 46.91%, 46.01%, and 53.32% for $(3d_{5/2}^{-1}5s_{1/2})_{3,2}$ and $(3d_{3/2}^{-1}5s_{1/2})_{1,2}$, respectively. The configuration-averaged BRs of the CDAD and DDAD processes are predicted to be 50.60% and 22.13%, resulting in the dominance of DAD, accounting for 72.73% of the Auger decay of $\text{Rb}^+(3d^{-1})$. The phenomenon of dominance of DAD was experimentally investigated by Koizumi *et al.* [34], who studied the relative ion yields Rb^{n+} ($n = 1-3$) of the Auger decay of the $3d$ hole states of $3d^94s^24p^65snp$ ($n = 5-6$) for atomic Rb. These authors observed that the production of DAD (Rb^{2+}) are dominant among the singly, doubly and triply charged ions.

To explain the extremely large BR of DAD, we propose that the outermost $5s$ electron is the physical origin. We compare Rb with its neighboring element Kr, which has a ground configuration of $4s^24p^6$, but no outermost $5s$ electrons. This comparison is shown in Table VI. For $\text{Kr}^+(3d^{-1})$, the BR of the DAD processes has been reported to be $32(\pm 4)\%$ [35], $30((\pm)1)\%$ [36], 26% [37], and 25% [38] experimentally and has been theoretically predicted to be 33.2% [23]. As mentioned above, the DAD BRs of $\text{Rb}^+(3d^{-1})$ are much larger than those of $\text{Kr}^+(3d^{-1})$.

With the same $3d$ initial hole in both $\text{Kr}^+(3d^{-1})$ and $\text{Rb}^+(3d^{-1})$ but one extra $5s$ electron in $\text{Rb}^+(3d^{-1})$, the Auger decay of $\text{Rb}^+(3d^{-1})$ is remarkably different from that of $\text{Kr}^+(3d^{-1})$. One big difference appears in the CDAD processes, where the BR of $\text{Rb}^+(3d^{-1})$ (50.6%) is triple that of $\text{Kr}^+(3d^{-1})$ (16.6%). Another difference appears in the

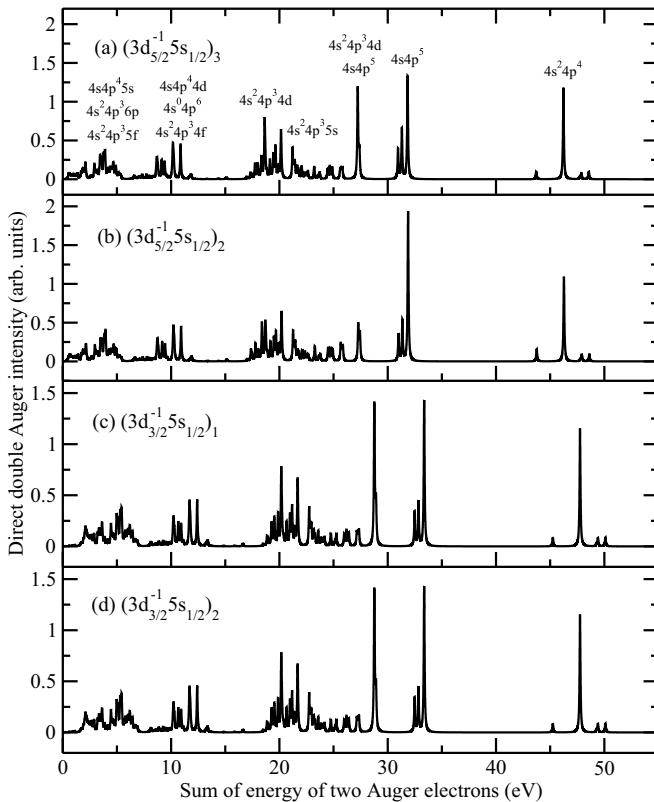


FIG. 4. Direct double Auger decay electron spectra of $(3d_{5/2}^{-1}5s_{1/2})_3$ (a), $(3d_{5/2}^{-1}5s_{1/2})_2$ (b), $(3d_{3/2}^{-1}5s_{1/2})_1$ (c), and $(3d_{3/2}^{-1}5s_{1/2})_2$ (d).

TABLE VI. Rates (s^{-1}) and BRs (in percent %) of the SAD, DDAD, CDAD, and DAD of $Rb^+(3d^{-1})$ levels. The BRs of DDAD and CDAD are defined as A_{DDAD}^2/A and A_{CDAD}^2/A , where A is the total decay rate obtained by summing the SAD rate and DDAD rate. The BR of DAD is a summation of that of DDAD and CDAD. For comparison, the results of $Kr^+(3d^{-1})$ [23] are also given. The last line of each ion shows the configuration averaged results. Figures in square brackets indicate powers of ten.

Atom	Initial level	Energy	SAD Rate	DDAD		CDAD		DAD	
				Rate	BR	Rate	BR	Rate	BR
Rb^+	$(3d_{5/2}^{-1}5s_{1/2})_3$	113.2	1.246[14]	3.459[13]	21.73	8.480[13]	53.26	1.194[14]	74.99
	$(3d_{5/2}^{-1}5s_{1/2})_2$	113.3	1.248[14]	3.506[13]	21.94	7.497[13]	46.91	1.100[14]	68.85
	$(3d_{3/2}^{-1}5s_{1/2})_1$	114.7	1.205[14]	3.481[13]	22.42	7.146[13]	46.01	1.063[14]	68.43
	$(3d_{3/2}^{-1}5s_{1/2})_2$	114.7	1.205[14]	3.544[13]	22.72	8.316[13]	53.32	1.186[14]	76.02
	$3d^{-1}5s$	113.8	1.230[14]	3.489[13]	22.13	7.876[13]	50.60	1.136[14]	72.73
Kr^+	$3d_{5/2}^{-1}$	79.1	1.367[14]	2.613[13]	16.1	2.693[13]	16.5	5.306[13]	32.6
	$3d_{3/2}^{-1}$	80.3	1.345[14]	2.796[13]	17.2	2.732[13]	16.8	5.528[13]	34.0
	$3d^{-1}$	79.6	1.358[14]	2.686[13]	16.5	2.709[13]	16.6	5.395[13]	33.2

DDAD processes, where the BR of $Rb^+(3d^{-1})$ is higher than that of $Kr^+(3d^{-1})$. The averaged-configuration of BR of the DDAD processes is predicted to be 22.13% for $Rb^+(3d^{-1})$, which is larger than the value of 16.5% for $Kr^+(3d^{-1})$. The larger DDAD probability of $Rb^+(3d^{-1})$ is due to the existence of the $5s$ electron. In the present work, we calculated the DDAD rates based on knock-out and shake-off mechanisms. As demonstrated in our previous work [22–24], the knock-out mechanism usually dominates the DDAD processes, while the shake-off mechanism is usually orders of magnitude smaller. As shown in Eqs. (2) and (3), the rates contributed by the knock-out mechanism are determined by the electron impact ionization cross sections of the second step of Auger decay. As shown in Fig. 5, the electron impact ionization cross-sections of the $5s$ electron in Rb^{2+} is larger than that of the $4p$ electron in Kr^{2+} .

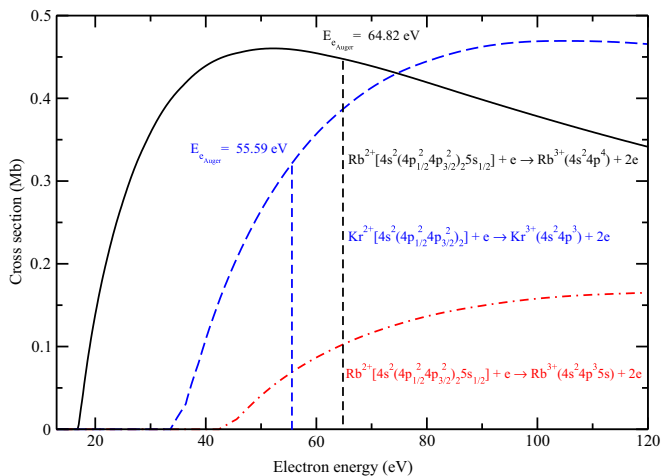


FIG. 5. Electron impact ionization cross sections from Rb^{2+} ($4s^2 4p_{1/2}^2 4p_{3/2}^2 5s_{1/2}$) to final configurations of Rb^{3+} ($4s^2 4p^4$) (black solid line) and Rb^{3+} ($4s^2 4p^3 5s$) (red dashed-dotted line), and $(4s^2 4p_{1/2}^2 4p_{3/2}^2)_2$ of Kr^{2+} to final configurations Kr^{3+} ($4s^2 4p^3$) (blue dashed line). The energies of Auger electrons are marked in black and blue vertical dashed lines for Rb and Kr, respectively.

IV. CONCLUSION

We theoretically investigated the complete Auger decay pathways, including single and double processes of $Rb^+(3d^{-1})$ by utilizing the distorted wave approximation. The DDAD rates are computed using the theoretical framework of the separation of knock-out and shake-off mechanisms. The lifetime of single Auger decay is predicted to be 81.0 meV, which agreed well with the experimental value of 79.0 meV. Our calculated SAD electron spectra make good agreement with previous theoretical results and reasonably explain experimental results. For the Auger decay of the $3d^{-1}$ hole state, it is generally believed that the dominant channels of SAD should be levels belonging to configurations of $4s^2 4p^4 5s$, $4s 4p^5 5s$, and $4s^0 4p^6 5s$. Here we predict that the strongest configuration originates from $4s^2 4p^3 4d 5s$, which accounts for 36.3% of the total decay rate. The reason for the strongest Auger decay channels originating from the levels of $4s^2 4p^3 4d 5s$, is due to the much stronger overlapping of the wave functions among the $4d$ and $5s$ electrons and continuum electron compared with that of the $4s$ and $4p$ electrons. The levels of configuration $4s^2 4p^3 4d 5s$ can further decay to Rb^{3+} , resulting in a high fraction of cascade double Auger decay. The branching ratios of cascade and direct double Auger decay are predicted to be 50.60% and 22.13%, resulting in the dominance of double Auger decay with a fraction of 72.73%. Compared with the Auger decay of $Kr^+(3d^{-1})$, the branching ratio of DDAD of $Rb^+(3d^{-1})$ is 37% higher. The higher probability of DDAD in Rb is due to the $5s$ electron in $Rb^+(3d^{-1})$, which has a larger electron impact ionization cross section than Kr in the second step of the knock-out mechanism. This work deserves further experiments to verify the dominance of double Auger decay in $Rb^+(3d^{-1})$.

ACKNOWLEDGMENTS

This work is supported by the National Key R&D Program of China under the Grant No. 2017YFA0403202, by Science Challenge Project No. TZ2018005 and the National Natural Science Foundation of China under Grants No. 11674394 and 11674395.

- [1] T. A. Carlson and M. O. Krause, Experimental Evidence for Double Electron Emission in an Auger Process, *Phys. Rev. Lett.* **14**, 390 (1965).
- [2] J. Viefhaus, S. Cvejanović, B. Langer, T. Lischke, G. Prümper, D. Rolles, A. V. Golovin, A. N. Grum-Grzhimailo, N. M. Kabachnik, and U. Becker, Energy and Angular Distributions of Electrons Emitted by Direct Double Auger Decay, *Phys. Rev. Lett.* **92**, 083001 (2004).
- [3] P. Lablanquie, L. Andric, J. Palaudoux, U. Becker, M. Braune, J. Viefhaus, J. H. D. Eland, and F. Penent, Multielectron spectroscopy: Auger decays of the argon 2p hole, *J. Electron Spectrosc. Relat. Phenom.* **156**, 51 (2007).
- [4] Y. Hikosaka, P. Lablanquie, F. Penent, J. Palaudoux, L. Andric, K. Soejima, E. Shigemasa, I. H. Suzuki, M. Nakano, and K. Ito, Energy Correlation Among three Photoelectrons Emitted in Core-Valence-Valence Triple Photoionization of Ne, *Phys. Rev. Lett.* **107**, 113005 (2011).
- [5] A. Müller, A. Borovik, T. Buhr, J. Hellhund, K. Holste, A. L. D. Kilcoyne, S. Klumpp, M. Martins, S. Ricz, J. Viefhaus, and S. Schippers, Observation of a Four-Electron Auger Process in Near-K-Edge Photoionization of Singly Charged Carbon Ions, *Phys. Rev. Lett.* **114**, 013002 (2015).
- [6] A. Müller, A. Borovik, T. Buhr, J. Hellhund, K. Holste, A. L. D. Kilcoyne, S. Klumpp, M. Martins, S. Ricz, J. Viefhaus, and S. Schippers, Observation of four-electron Auger processes, *J. Phys.: Conf. Ser.* **635**, 012033 (2015).
- [7] C. W. Hogle, X. M. Tong, L. Martin, M. M. Murnane, H. C. Kapteyn, and P. Ranitovic, Attosecond Coherent Control of Single and Double Photoionization in Argon, *Phys. Rev. Lett.* **115**, 173004 (2015).
- [8] M. Y. Amusia, I. S. Lee, and V. A. Kilin, Double Auger decay in atoms: Probability and angular distribution, *Phys. Rev. A* **45**, 4576 (1992).
- [9] M. S. Pindzola, F. Robicheaux, and J. P. Colgan, Double autoionization of hollow-atom states, *Phys. Rev. A* **72**, 022709 (2005).
- [10] M. S. Pindzola, F. Robicheaux, and J. P. Colgan, Double autoionization of He-($2s^2 2p^2 P$), *Phys. Rev. A* **73**, 062720 (2006).
- [11] H. Aksela, S. Aksela, R. Lakanen, J. Tulkki, and T. Åberg, Initial-and final-state correlation in the valence-shell Auger spectrum of Rb, *Phys. Rev. A* **42**, 5193 (1990).
- [12] J. Keskinen, P. Lablanquie, F. Penent, J. Palaudoux, L. Andric, D. Cubaynes, J.-M. Bizau, M. Huttula, and K. Jänkälä, Initial-state-selected MNN Auger spectroscopy of atomic rubidium, *Phys. Rev. A* **95**, 043402 (2017).
- [13] G. Goldsztejn, R. Püttner, L. Journel, R. Guillemin, O. Travnikova, B. Cunha de Miranda, I. Ismail, S. Carniato, P. Selles, D. Céolin, A. F. Lago, R. Feifel, P. Lablanquie, F. Penent, M. N. Piancastelli, M. Simon, T. Marchenko, Experimental and theoretical study of the double-core-hole hypersatellite Auger spectrum of Ne, *Phys. Rev. A* **96**, 012513 (2017).
- [14] Y. Li, L. Liu, C. Gao, J. Zeng, and J. Yuan, Auger decay including direct double processes of K-shell hollow states of Ne⁺ and the related hypersatellite radiative transitions, *J. Electron Spectrosc. Relat. Phenom.* **226**, 26 (2018).
- [15] P. Lablanquie, M. A. Khalal, L. Andric, J. Palaudoux, F. Penent, J.-M. Bizau, D. Cubaynes, K. Jänkälä, Y. Hikosaka, K. Ito, K. Bučar, and M. Žitnik, Multi-electron coincidence spectroscopy: Triple Auger decay of Ar 2p and 2s holes, *J. Electron Spectrosc. Relat. Phenom.* **220**, 125 (2017).
- [16] J. Palaudoux, P. Lablanquie, L. Andric, K. Ito, E. Shigemasa, J. H. D. Eland, V. Jonauskas, S. Kučas, R. Karazija, and F. Penent, Multielectron spectroscopy: Auger decays of the krypton 3d hole, *Phys. Rev. A* **82**, 043419 (2010).
- [17] E. Andersson, S. Fritzsche, P. Linusson, L. Hedin, J. H. D. Eland, J.-E. Rubensson, L. Karlsson, and R. Feifel, Multielectron coincidence study of the double Auger decay of 3d-ionized krypton, *Phys. Rev. A* **82**, 043418 (2010).
- [18] Y. Hikosaka, P. Lablanquie, F. Penent, T. Kaneyasu, E. Shigemasa, J. H. D. Eland, T. Aoto, and K. Ito, Single, double, and triple Auger decay of the Xe 4p core-hole states, *Phys. Rev. A* **76**, 032708 (2007).
- [19] K. Jänkälä, J. Schulz, M. Huttula, A. Caló, S. Urpelainen, S. Heinäsmäki, S. Fritzsche, S. Svensson, S. Aksela, and H. Aksela, Effects of initial-state laser excitation on inner-shell photoionization and Auger decay of Rb, *Phys. Rev. A* **74**, 062704 (2006).
- [20] Kh. A. Inoyatov, A. Kovalík, L. L. Perevoshchikov, D. V. Filosofov, D. Vénos, B. Q. Lee, J. Ekman, and A. Baimukhanova, The KLM+KLN Auger electron spectrum of rubidium in different matrices, *J. Phys. B: At. Mol. Phys.* **50**, 155001 (2017).
- [21] M. F. Gu, The flexible atomic code, *Can. J. Phys.* **86**, 675 (2008).
- [22] P. Liu, J. Zeng, and J. Yuan, A practical theoretical formalism for atomic multielectron processes: direct multiple ionization by a single auger decay or by impact of a single electron or photon, *J. Phys. B: At. Mol. Phys.* **51**, 075202 (2018).
- [23] J. Zeng, P. Liu, W. Xiang, and J. Yuan, Complete Auger decay pathways of Kr 3d⁻¹ hole levels including direct double processes, *J. Phys. B: At. Mol. Phys.* **46**, 215002 (2013).
- [24] J. Zeng, P. Liu, W. Xiang, and J. Yuan, Level-to-level and total probability for Auger decay including direct double processes of Ar 2p⁻¹ hole states, *Phys. Rev. A* **87**, 033419 (2013).
- [25] M. S. Pindzola and D. C. Griffin, Double Auger processes in the electron-impact ionization of lithiumlike ions, *Phys. Rev. A* **36**, 2628 (1987).
- [26] F. A. Parpia, C. Froese Fischer, and I. P. Grant, GRASP92: A package for large-scale relativistic atomic structure calculations, *Comput. Phys. Commun.* **94**, 249 (1996).
- [27] P. Jönsson, X. He, C. Froese Fischer, and I. P. Grant, The grasp2K relativistic atomic structure package, *Comput. Phys. Commun.* **177**, 597 (2007).
- [28] S. Fritzsche, Ratip-a toolbox for studying the properties of open-shell atoms and ions, *J. Electron Spectrosc. Relat. Phenom.* **114**, 1155 (2001).
- [29] S. Fritzsche, The RATIP program for relativistic calculations of atomic transition, ionization and recombination properties, *Comput. Phys. Commun.* **183**, 1525 (2012).
- [30] J. Zeng, J. Yuan, and Q. Lu, Photoionization of O III low-lying states: autoionization resonance energies and widths of some 1s-2p excited states, *J. Phys. B: At. Mol. Phys.* **34**, 2823 (2001).
- [31] J. Zeng and J. Yuan, Photoionization of Be-like neon (Ne VII) from the low-lying states: Energies, widths, branching ratios, and oscillator strengths of the 1s-2p resonances, *Phys. Rev. A* **66**, 022715 (2002).
- [32] J. Zeng, G. Dong, G. Zhao, and J. Yuan, The photoionization of Fe⁷⁺ and Fe⁸⁺ in the 2p-3d resonance energy region, *J. Phys. B: At. Mol. Phys.* **37**, 2529 (2004).

- [33] A. Kramida, Yu. Ralchenko, J. Reader, and NIST ASD Team (2018), NIST Atomic Spectra Database (ver. 5.6.1), [Online]. Available: <https://physics.nist.gov/asd> [September 18, 2019]. National Institute of Standards and Technology, Gaithersburg, MD.
- [34] T. Koizumi, T. Hayaishi, Y. Itikawa, Y. Sato, and A. Yagishita, Decay channels after the photoexcitation of 3d electrons in Rb and Sr studied by photoion yield spectra[J], *J. Phys. B: At. Mol. Phys.* **20**, 5393 (1987).
- [35] Y. Tamenori, K. Okada, S. Tanimoto, T. Ibuki, S. Nagaoka, A. Fujii, Y. Haga, and I. H. Suzuki, Branching ratios of multiply charged ions formed through photoionization of Kr 3d, 3p and 3s sub-shells using a coincidence technique, *J. Phys. B: At. Mol. Phys.* **37**, 117 (2004).
- [36] S. Brünken, Ch. Gerth, B. Kanngießer, T. Luhmann, M. Richter, and P. Zimmermann, Decay of the Ar $2s^{-1}$ and $2p^{-1}$ and Kr $3p^{-1}$ and $3d^{-1}$ hole states studied by photoelectron-ion coincidence spectroscopy, *Phys. Rev. A* **65**, 042708 (2002).
- [37] N. Saito and I. H. Suzuki, Double Auger Probabilities from Xe $4d_j$, Kr $3d_j$, and Ar $2p_j$ Hole States, *J. Phys. Soc. Japan* **66**, 1979 (1997).
- [38] E. Murakami, T. Hayaishi, A. Yagishita, and Y. Morioka, Multiple and partial photoionization cross sections in the Kr 3d ionization region, *Phys. Scr.* **41**, 468 (1990).